Flexible Superlubricity Unveiled in Sidewinding Motion of Individual Polymeric Chains

J. G. Vilhena,[1,2,*,§] Rémy Pawlak,[1,†,§] Philipp D'Astolfo,[1] Xunshan Liu,[3,4] Enrico Gnecco,[5] Marcin Kisiel,[1] Thilo Glatzel,[1] Rúben Pérez,[2,6] Robert Häner,[4] Silvio Decurtins,[4] Alexis Baratoff,[1] Giacomo Prampolini,[7] Shi-Xia Liu,[4] and Ernst Meyer[1,‡]

[1]*Department of Physics, University of Basel, Klingelbergstrasse 82, 4056 Basel, Switzerland*
[2]*Departamento de Física Teórica de la Materia Condensada, Universidad Autónoma de Madrid, E-28049 Madrid, Spain*
[3]*Department of Chemistry, Zhejiang Sci-tech University, 314423 Hangzhou, China*
[4]*Department of Chemistry, Biochemistry and Pharmaceutical Sciences, University of Bern, Freiestrasse 3, 3012 Bern, Switzerland*
[5]*Marian Smoluchowski Institute of Physics, Jagiellonian University, Lojasiewicza 11, 30-348 Krakow, Poland*
[6]*Condensed Matter Physics Center (IFIMAC), Universidad Autónoma de Madrid, E-28049 Madrid, Spain*
[7]*Istituto di Chimica dei Composti Organo Metallici, Consiglio Nazionale delle Ricerche (ICCOM-CNR), 56124 Pisa, Italy*

(Received 28 September 2021; revised 22 February 2022; accepted 19 April 2022; published 26 May 2022)

A combination of low temperature atomic force microcopy and molecular dynamic simulations is used to demonstrate that soft designer molecules realize a sidewinding motion when dragged over a gold surface. Exploiting their longitudinal flexibility, pyrenylene chains are indeed able to lower diffusion energy barriers via on-surface directional locking and molecular strain. The resulting ultralow friction reaches values on the order of tens of pN reported so far only for rigid chains sliding on an incommensurate surface. Therefore, we demonstrate how molecular flexibility can be harnessed to realize complex nanomotion while retaining a superlubric character. This is in contrast with the paradigm guiding the design of most superlubric nanocontacts (mismatched rigid contacting surfaces).

DOI: 10.1103/PhysRevLett.128.216102

Controlling friction is arguably one of the oldest quests of our civilization [1,2]. From wetting the desert sands to transport the building block of ancient Egyptian wonders [3] down to micro-electro-mechanical devices [4], a better understanding of this ubiquitous phenomena has closely followed our technological advancement. Thus, the realization of a near frictionless sliding contact [5,6], known as structural superlubricity, has attracted a widespread interest [4,7–12]. Structural superlubricity emerges from a lattice mismatch or misalignment between two sliders in direct contact ultimately preventing them from interlocking—thus reducing energy barriers related to lateral motion. Hence, superlubric designs depend on the sliders' rigidity [4] to prevent the geometrical registry naturally favored by the interaction between contacts—a stringent criteria often leading to its demise [4]. Concomitantly, recent trends in nanodevices depart from the use of rigid elements to embrace bioinspired designs [13], where flexibility is pivotal for the device function [13–16]. Here we explicitly challenge the importance of rigidity in superlubricity by recognizing ultralow friction in the sidewinding [17–19] motion of a molecular system. We also show how *flexolubricity* is achieved by means of complex on-surface dynamics, which goes well beyond rectilinear nanomotion and paves the way for improved energy dissipation schemes in novel molecular architectures and future nanobionic devices.

Purposely synthesized 2,7-dibromopyrene monomers (DBP) are evaporated onto a clean Au(111) crystal and subsequently polymerized *via* Ullmann coupling. The resulting flexible chains are imaged using a combined scanning tunneling microscope (STM) and atomic force microscope (AFM) operated at low temperature (4.8 K) and ultra-High-Vacuum (UHV) [20]. The chain manipulation is achieved thanks to a stable tip-molecule bound formed by pressing the AFM tip against one end of a chain [yellow dot in Fig. 1(g)] [7,32–34]. During the manipulation, the tip kept oscillating at an amplitude of 50 pm and eigenfrequency f_0 of the supporting qPlus tuning fork. The measured frequency shifts Δf directly relates to the gradient of the normal force acting on the tip, k_{eff} [32,35]. Although not trivially connected to friction forces, k_{eff} informs [4,7,9] about the dynamics (e.g., slip length, hysteresis,…) and it may be computed using all atom molecular dynamics (MD) [7,33,34]. Here, an atomic detailed understanding on the link between flexibility and superlubricity is provided by MD simulations of a 10-unit pyrenylene chain (polymer of 10 DBP units) adsorbed along $[11\bar{2}]$ crystallographic direction of a Au(111) surface. The chain is then manipulated (first lifted, then sled along $[11\bar{2}]$) at a speed of 0.1 m/s whilst maintaining a 5 K temperature thanks to a Langevin thermostat [36]. Beyond the atomic details, MD also provided friction and normal forces, and the gradient of

 © 2022 American Physical Society

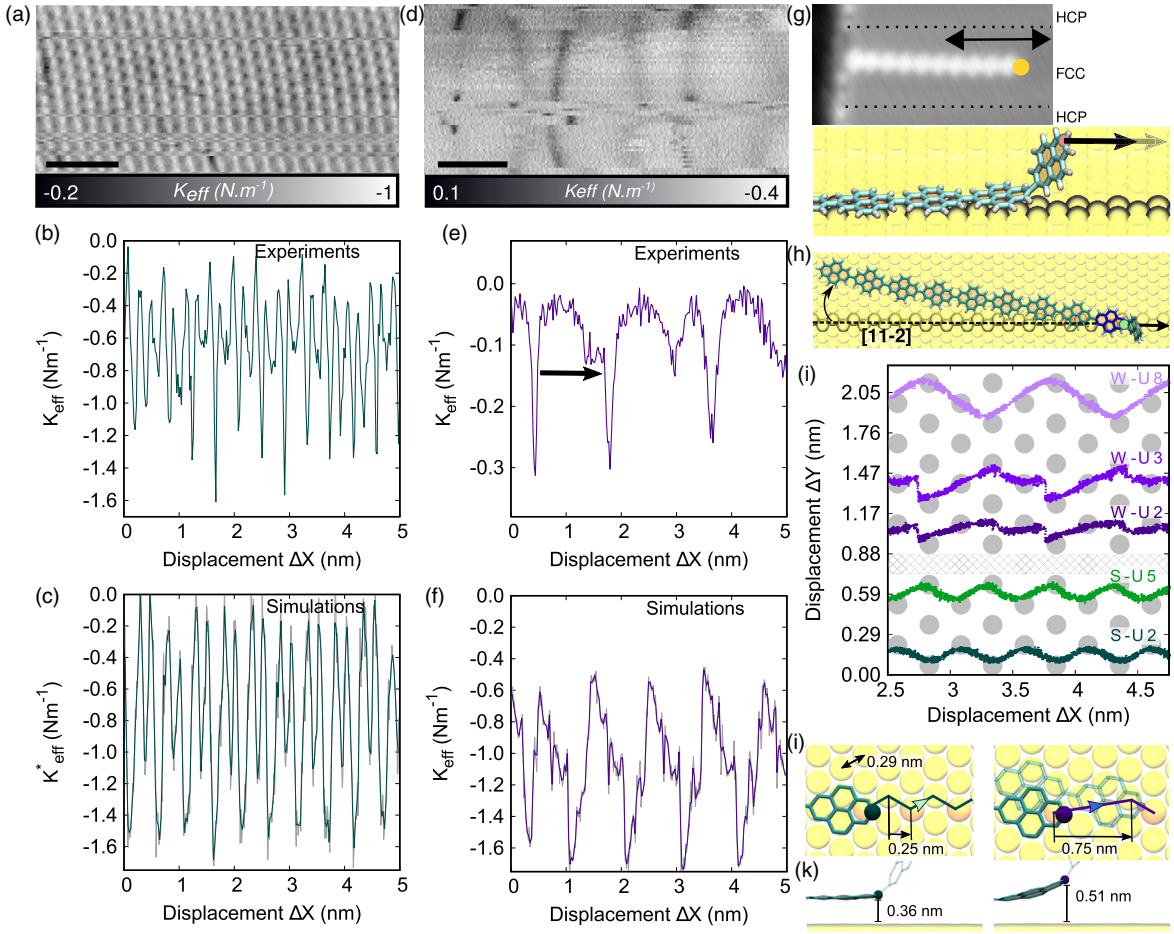

FIG. 1. Slithering dynamics of a deca-pyrenylene on Au(111). Experimental stiffness maps $k_{\mathrm{eff}}(x, y)$ (a),(d) representative trace (b),(e) and corresponding simulation results (c),(f) obtained during the sliding at different heights, i.e., in strong contact (a)–(c) and in a weak contact (d)–(f) regimes. (g) Initial configuration of the polymer before sliding, and schematic side view representation. (h) Representative configuration of the deca-pyrenylene during sliding. (i) Paracarbon atom trajectory of the second and fifth units for the strong contact regime (S-U2, S-U5 shown in green) and trajectories of the second, third, and eighth units for the weak contact regime (W-U2, W-U3, W-U8 shown in purple). Top (j) and side (k) views of intermediate sliding stages in the strong (left) and weak (right) contact regimes.

the latter directly relates to experiments data (i.e., k_{eff}). MD simulations were carried out using GROMACS-2018.2 [21], a purposely derived quantum mechanical force field (QM-FF) for the pyrelene chain [20], and GolP [22] FF for the molecule-gold interaction.

Figure 1 shows a 10-unit pyrenylene chain initially aligned along the $[11\bar{2}]$ direction of Au(111) prior to manipulation. Conveniently, this spontaneous adsorption alignment [33] allows manipulating the molecule without crossing a Au(111) herringbone [7]. After its synthesis, the molecule is lifted from the surface up to a well-defined height Z and driven for 10 nm along the same $[11\bar{2}]$ direction. Figures 1(a) and 1(d) show two representative k_{eff} maps obtained by driving the chain head along a series of lines parallel to $[11\bar{2}]$ at low and high tip-sample separations (Z), respectively,—henceforth referred to as strong (low-Z) and weak (high-Z) contact regimes (data at other heights is provided in Figs. S1–S2 of Ref. [20]).

The strong contact regime is characterized by a k_{eff} repetition distance of $d_{\mathrm{SC}} = 0.22$ nm [Fig. 1(b)]. Prior works [7,32–34] allow us to associate k_{eff} increase or decrease with pinning or unpinning events of the molecule to the substrate. However, the measured slip distance ($d_{\mathrm{SC}} \sim 0.22$ nm) is much smaller than any substrate's periodicity (i.e., $d_{\mathrm{Au-Au}} = 0.28$ nm Au-Au distance and $d_{[11\bar{2}]} = 0.5$ nm the lattice periodicity along $[11\bar{2}]$). The results of all-atom MD simulations are in quantitative agreement with experiments [Fig. 1(c)]. Simulations confirm that k_{eff} maxima or minima are associated with stick or slip events and the short sliding period, i.e., $d_{\mathrm{SC}} < d_{\mathrm{Au-Au}}$, provides a distinct signature of a nontrivial zigzag motion shown in the Supplemental Material, video S1 [20].

When the pyrenylene head is pulled, the entire chain twists its longitudinal axis by 10°–13° with respect to the sliding direction [Fig. 1(h)]. At the same time, each pyrenylene zigzags forward on the surface by moving only

along compact or superlubric directions [23] oriented at ±30° with the sliding direction—a process known as directional locking [4,24,25]. This is apparent in its on-surface trajectory [Figs. 1(i),1(j)], where one observes that initially the monomer moves away from the sliding-axis only to return in the subsequent slip event, but now one crystallographic position ahead along the sliding direction (i.e., $d_{[11\bar{2}]} = 0.5\ \text{nm} \approx 2 \times d_{SC}^{MD}$). This intermediate off-axis slide event, not only explains the small slip distance d_{SC} but it also proves the existence of a molecular undulation—in agreement with prior theoretical predictions on other chains [12]. Moreover, this sinusoidal motion is not a rigid one, instead, it is a dynamic concerted motion throughout the chain with a large phase shift between neighboring units [see in Fig. 1(i) how the nth unit oscillates in antiphase with the $(n+3)$-th]. In the following we explain how this complex motion (that partially resembles snake sidewinding motion [17–19]) allows the chain to effectively mitigate static and sliding friction.

In the weak contact regime, the experimental k_{eff} map [Figs. 1(d) and 1(e)] changes substantially, with short stick-slip events being replaced by long and less regular jumps. The simulation results in Fig. 1(f), show a k_{eff} periodicity of $d_{WC} \sim 1$ nm—similarly to experiments [arrow in Fig. 1(e)]. Moreover, each unit advances in a specific way, and trajectories of consecutive units are not simply shifted as in the case of strong contact [see Fig. 1(i)]. Therefore, a small change of pyrenylene head height (of 0.15 nm from the strong to weak contact regime) alter the dynamics of a 9 nm long chain all the way to its tail. This effect arises from the torsion between consecutive units, that in the gas phase favors a 40° angle (see Fig. S3 [20])—opposed to the ≈0° angle of the adsorbed pyrenylene chain. In the strong-contact regime the second unit lays flat and the U2–U3 torsion is nearly zero. By lifting the second unit 0.15 nm, the U2–U3 angle is no longer zero and the torsion between these units pushes the molecule away from the sliding axis (Fig. S3 [20]). Thus, via a small height change one enables or disables an internal coordinate of the molecule, which, in turn, allows us to alter the dynamics of the chain as a whole (Fig. S3 [20]). Interestingly, a comparable effect (so-called "rolling") is also found in snakes [18].

It is also instructing to investigate how molecular flexibility, and consequent sideway-zigzag motion, play out in a backward manipulation [Fig. 2(a)]. In Figs. 2(b) and 2(c) we compare experimental and simulated variations of k_{eff} when the pyrenylene chain is pulled forth and back in the strong contact regime. In contrast to superlubric graphene-nanoribbon (GNR) sliding over Au(111) [7], here only a small hysteresis is observed, suggesting that the sliding occurs even more smoothly than in rigid GNRs [7]. Moreover, a close inspection of the trajectory (see Supplemental Material [20], movie 3) reveals that (i) in spite of its high in-plane flexibility, the molecule slides back with the tail moving ahead [Fig. 2(c)]; and (ii) the

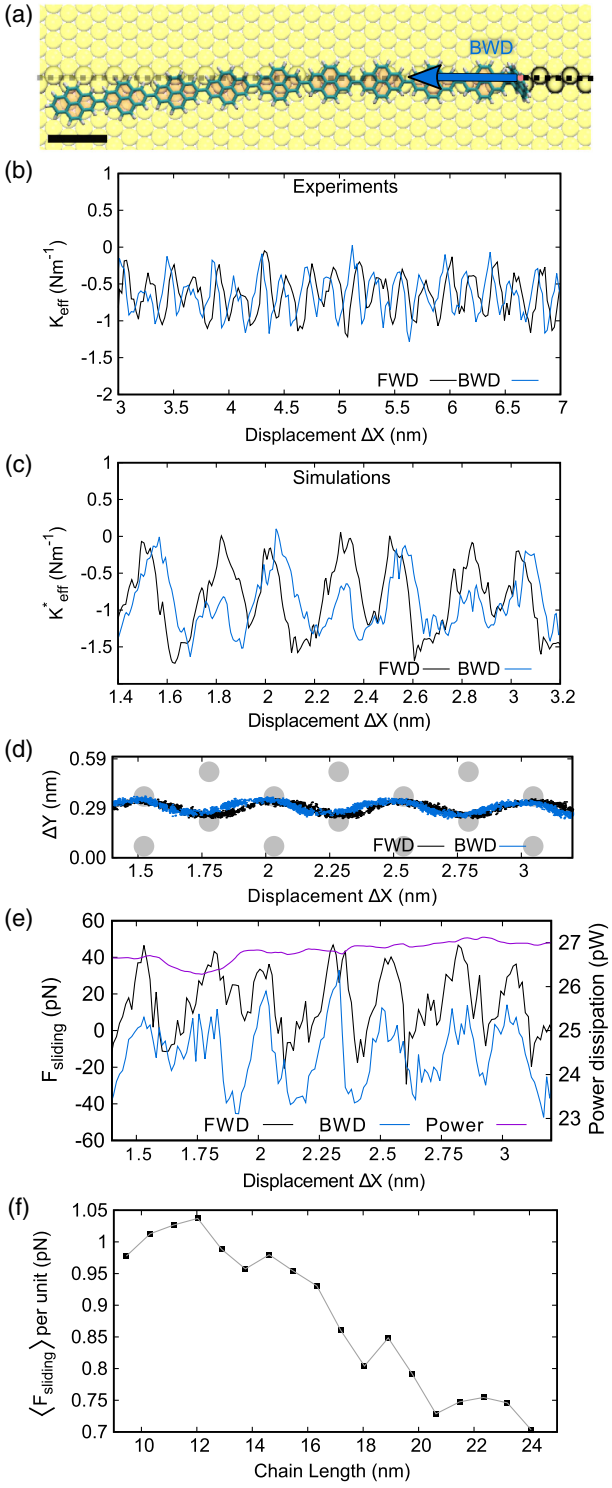

FIG. 2. Backward sliding and apparent flexible superlubricity. (a) Representative snapshot of the backward motion of the deca-pyrenylene. (b),(c) Forward (FWD) and backward (BWD) $k_{eff}(x)$ obtained in experiments and simulations, respectively. (d) Unit 2 para-carbon atom trajectory of the deca-pyrenylene FWD/BWD sliding. (e) FWD/BWD deca-pyrenylene sliding force traces with the corresponding power dissipation. (f) Average friction per unit as a function of the poly-pyrenylene chain length.

wavy motion at the single pyrenylene level is preserved regardless of the sliding direction, i.e., forward or backward. Moreover, the motion of the first contact unit is almost identical in both directions [Fig. 2(d)], consistently with the small k_{eff} hysteresis.

From the lateral force in Fig. 2(e) we compute a static friction of $F_{\mathrm{stat}} = \sim 40$ pN, which is comparable to superlubic GNR ($F_{\mathrm{stat}}^{\mathrm{GNR}} \sim 35$ pN) sliding along a more packed or lubric [23] direction. Therefore our results show that ultralow friction is not exclusive to rigid sliders [7–9,11] as it may also be realized in flexible ones. Moreover, the slider rigidity has also guided most of today's superlubric designs [4,7,8,10,11], as it prevents establishing a geometric registry with the surface lattice—thus canceling friction forces. One hallmark feature of standard superlubric contacts is the asymptotically vanishing friction per unit area of contact—a property verified in GNR with lengths up to 25 nm [7]. In Fig. 2(f), we represent the simulated average sliding friction as a function of the number of pyrene units. As in superlubric GNRs, the sliding friction is found to decrease with increasing chain length. A similar conclusion holds for static friction (Fig. S4 [20]), meaning that the energy required to unpin a given chain atom is reduced by increasing pyrenylene chain length. In a chain capable of improving its registry in every slip event—ergo incompatible with conventional structural-superlubricity [4,7,8,10,11]—such force cancellation must stem from internal molecular forces.

In the following we thus focus on the incommensurability between polycyclic-aromatic-hydrocarbon chains and Au(111). It causes two major effects: (i) mechanical stress due to surface-templated bending, and (ii) "asynchronous" excitation or deexcitation of internal degrees of freedom (DOF) while sliding. The first effect is revealed by the angle between the first and second adsorbed units in the strong contact regime [Fig. 3(a)]. This angle oscillates between two nonequilibrium values (±0.75°), corresponding to initial and intermediate bent states. Consequently, the chain is constantly under strain except when it slips from one configuration to another [highlighted by a purple dashed line in Figs. 3(a)–3(c)]. The second effect is less local, as exemplified in Fig. 3(a) when comparing the bend angles of the U2–U3 and U5–U6 junctions. Upon sliding, these angles oscillate almost in antiphase thus canceling out much of the lateral forces. However, two perfectly synchronized bending events throughout the whole chain are never observed, regardless the chain length (Fig. S5 [20]). Therefore, the chain is constantly under strain while sliding with internal DOF being continuously excited or deexcited. As a result, the chain length can be virtually increased without proportionally increasing the work required to bend all units (see Supplemental Material [20], note 2 for details). In other words, the incommensurability between pyrenylene and Au(111), induces local bending with spatially incoherent phase shifts among the pyrenylene units inasmuch as atomic positions of substrate and slider never match in structural superlubricity [4,7,8,10,11].

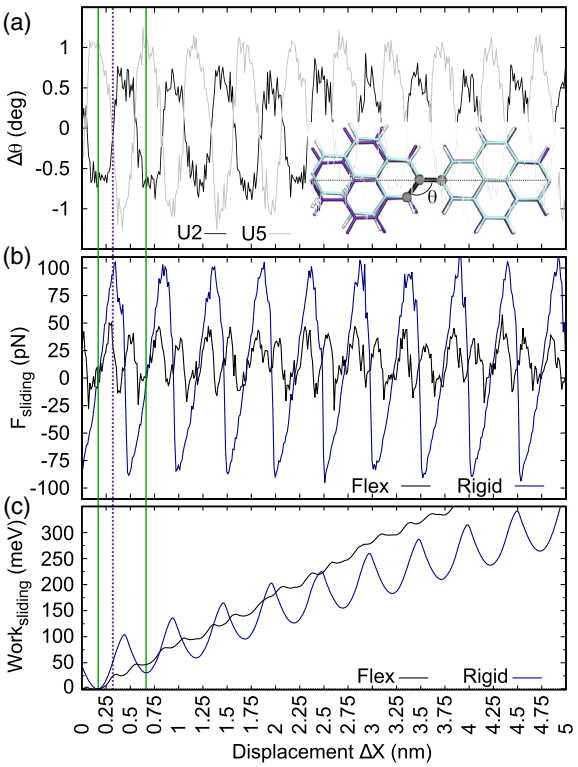

FIG. 3. Correlation between excitation of bending angles, slip dynamics, and energy dissipation of a deca-pyrenylene sled over Au(111). (a) Evolution of $\Delta\theta$ during sliding [U2 stands for unit 2 and 3, and U5 for unit 5 and 6—trajectories are shown in Fig. 1(i)]. In the inset, the bending angle ($\Delta\theta$) between the second and third unit is represented (purple or cyan represent a straight or bent configuration during slip or stick). (b) Evolution of the friction force (c) and work required to displace the chain during the sliding dynamics.

The role of internal DOF is best seen when comparing friction forces of both flexible and rigid pyrenylene chains sled over Au(111) [Fig. 3(b)]. Three major differences are observed, namely, flexible sideway-zigzag motion: (i) decreases the slip length; (ii) substantially decreases the static-friction force; and (iii) has a higher average-friction force. Regarding the slip length, the rigid chain, lacking the ability to bend, can only slip a distance of $2 \times d_{\mathrm{SC}}$ along the driving direction. From here it follows the first important consequence of molecular flexibility, i.e., to break down on-surface motion into smaller slip events with smaller energy barriers. The connection with the second observation is straightforward: smaller slip events require unpinning a smaller number of atoms, thus requiring lower forces to initiate the motion. Furthermore, the total strain stored in a flexible molecule emerging from the surface templated bending, cannot be recovered in the rigid case. As shown in Fig. 3(a), the bending strain decreases at the onset of slip events only, when the chain is partially

straightened. Thus, bending energy allows us, on the one hand, to reduce the amount of work required to unpin pyrenylene atoms, and, on the other, to recover part of the slip kinetic energy as molecular strain after the slip (see other energy components in Fig. S7 [20]). Nevertheless, internal DOF excitation will result in vibrations that couple to the substrate and increase energy dissipation, as shown in Fig. 3(c). In the rigid case, after each slip event one recovers a substantial amount of the energy spent to initiate the motion—at odds with the flexible chain, where less than 10% is recovered. To sum up, the molecular flexibility reduces diffusion energy barriers by introducing new local minima and controlled release or storage of molecular strain. Therefore, flexible chains might outperform rigid ones in nanoscale displacements since their diffusion energy barriers are substantially reduced.

In conclusion, we have shown how molecular flexibility can be harnessed to realize complex nanoscale motion, while retaining superior tribological performance. The sideway-zigzag motion of the chains, the ability to change their trajectory by an incremental chain-head lift, its flexible-superlubric character, unveiled a rich phenomenology showcasing a great potential in chemically tailoring tribological properties of molecules composing the increasing number of nanomechanical systems [13,15,16]. Most importantly, our results demonstrate how superlubricity can be realized in flexible contacts—contrary to the pervasive paradigm reliant on mismatched rigid contacting surfaces.

The work is supported by Swiss National Science Foundation (SNF Grant No. CRSK-2 190731/1), Swiss Nanoscience Institute (SNI), European Research Council (ERC), under the European Unions Horizon 2020 research and innovation program (Grant Agreement No. 834402), the FET-Open Programme (Grant No. 828966), MSC Action DLV-795286, COST Action MP1303, Spanish Research Agency (Projects No. MDM-2014-0377, No. MAT2014-54484-P, No. MAT2017-83273-R, No. PID2020-113722RJ-I00, the Spanish CM "Talento Program" Project No. 2020-T1/ND-20306), and the Jagiellonian University (SciMat Grant No. U1U/P05/NO/01.05).

*Corresponding author.
guilhermevilhena@gmail.com
†Corresponding author.
remy.pawlak@unibas.ch
‡Corresponding author.
ernst.meyer@unibas.ch
§These two authors contributed equally.

[1] D. Dowson, *History of Tribology* (Addison-Wesley Longman Limited, Reading, MA, 1978).
[2] A. Vanossi, N. Manini, M. Urbakh, S. Zapperi, and E. Tosatti, Colloquium: Modeling friction: From nanoscale to mesoscale, Rev. Mod. Phys. **85**, 529 (2013).
[3] A. Fall, B. Weber, M. Pakpour, N. Lenoir, N. Shahidzadeh, J. Fiscina, C. Wagner, and D. Bonn, Sliding Friction on Wet and Dry Sand, Phys. Rev. Lett. **112**, 175502 (2014).
[4] A. Vanossi, C. Bechinger, and M. Urbakh, Structural lubricity in soft and hard matter systems, Nat. Commun. **11**, 4657 (2020).
[5] M. Hirano, K. Shinjo, R. Kaneko, and Y. Murata, Anisotropy of Frictional Forces in Muscovite Mica, Phys. Rev. Lett. **67**, 2642 (1991).
[6] J. M. Martin, C. Donnet, T. Le Mogne, and T. Epicier, Superlubricity of molybdenum disulphide, Phys. Rev. B **48**, 10583 (1993).
[7] S. Kawai, A. Benassi, E. Gnecco, H. Söde, R. Pawlak, X. Feng, K. Müllen, D. Passerone, C. A. Pignedoli, P. Ruffieux, R. Fasel, and E. Meyer, Superlubricity of graphene nanoribbons on gold surfaces, Science **351**, 957 (2016).
[8] Y. Song, D. Mandelli, O. Hod, M. Urbakh, M. Ma, and Q. Zheng, Robust microscale superlubricity in graphite/hexagonal boron nitride layered heterojunctions, Nat. Mater. **17**, 894 (2018).
[9] O. Hod, E. Meyer, Q. Zheng, and M. Urbakh, Structural superlubricity and ultralow friction across the length scales, Nature (London) **563**, 485 (2018).
[10] D. Dietzel, J. Brndiar, I. Štich, and A. Schirmeisen, Limitations of structural superlubricity: Chemical bonds versus contact size, ACS Nano **11**, 7642 (2017).
[11] S. Zhang, T. Ma, A. Erdemir, and Q. Li, Tribology of two-dimensional materials: From mechanisms to modulating strategies, Mater. Today **26**, 67 (2019).
[12] W. Ouyang, D. Mandelli, M. Urbakh, and O. Hod, Nanoserpents: Graphene nanoribbon motion on two-dimensional hexagonal materials, Nano Lett. **18**, 6009 (2018).
[13] L. Zhang, V. Marcos, and D. A. Leigh, Molecular machines with bio-inspired mechanisms, Proc. Natl. Acad. Sci. U.S.A. **115**, 9397 (2018).
[14] Z. Wang, J. Wang, J. Ayarza, T. Steeves, Z. Hu, S. Manna, and A. P. EsserKahn, Bio-inspired mechanically adaptive materials through vibration-induced crosslinking, Nat. Mater. **20**, 869 (2021).
[15] D. Peller, L. Z. Kastner, T. Buchner, C. Roelcke, F. Albrecht, N. Moll, R. Huber, and J. Repp, Sub-cycle atomic-scale forces coherently control a single-molecule switch, Nature (London) **585**, 58 (2020).
[16] D. Civita, M. Kolmer, G. J. Simpson, A. P. Li, S. Hecht, and L. Grill, Control of long-distance motion of single molecules on a surface, Science **370**, 957 (2020).
[17] H. C. Astley, C. Gong, J. Dai, M. Travers, M. M. Serrano, P. A. Vela, H. Choset, J. R. Mendelson, D. L. Hu, and D. I. Goldman, Modulation of orthogonal body waves enables high maneuverability in sidewinding locomotion, Proc. Natl. Acad. Sci. U.S.A. **112**, 6200 (2015).
[18] H. Marvi, C. Gong, N. Gravish, H. Astley, M. Travers, R. L. Hatton, J. R. Mendelson, H. Choset, D. L. Hu, and D. I. Goldman, Sidewinding with minimal slip: Snake and robot ascent of sandy slopes, Science **346**, 224 (2014).
[19] I. J. Yeaton, S. D. Ross, G. A. Baumgardner, and J. J. Socha, Undulation enables gliding in flying snakes, Nat. Phys. **16**, 974 (2020).
[20] See Supplemental Material at http://link.aps.org/supplemental/10.1103/PhysRevLett.128.216102, which

includes Refs. [21–31], Supplementary Figures S1–S7 and the captions for the Supplementary Movies SM1–SM3.

[21] M. J. Abraham, T. Murtola, R. Schulz, S. Pll, J. C. Smith, B. Hess, and E. Lindahl, Gromacs: High performance molecular simulations through multi-level parallelism from laptops to supercomputers, SoftwareX **1–2**, 19 (2015).

[22] S. C. F. Iori, R. Di Felice, and E. Molinari, GolP: An atomistic force-field to describe the interaction of proteins with Au(111) surfaces in WaterGolP: An atomistic force-field to describe the interaction of proteins with Au(111) surfaces in water, J. Comput. Chem. **30**, 1465 (2009).

[23] L. Gigli, N. Manini, A. Benassi, E. Tosatti, A. Vanossi, and R. Guerra, Graphene nanoribbons on gold: Understanding superlubricity and edge effects, 2D Mater. **4**, 045003 (2017).

[24] X. Cao, E. Panizon, A. Vanossi, N. Manini, and C. Bechinger, Orientational and directional locking of colloidal clusters driven across periodic surfaces, Nat. Phys. **15**, 776 (2019).

[25] F. Trillitzsch, R. Guerra, A. Janas, N. Manini, F. Krok, and E. Gnecco, Directional and angular locking in the driven motion of au islands on mos_2, Phys. Rev. B **98**, 165417 (2018).

[26] A. G. Crawford, Z. Liu, I. A. I. Mkhalid, M.-H. Thibault, N. Schwarz, G. Alcaraz, A. Steffen, J. C. Collings, A. S. Batsanov, J. A. K. Howard, and T. B. Marder, Synthesis of 2- and 2,7-functionalized pyrene derivatives: An application of selective c-h borylation, Chem. Eur. J. **18**, 5022 (2012).

[27] F. J. Giessibl, The qPlus sensor, a powerful core for the atomic force microscope, Rev. Sci. Inst. **90**, 011101 (2019).

[28] S. Páll, M. J. Abraham, C. Kutzner, B. Hess, and E. Lindahl, Tackling exascale software challenges in molecular dynamics simulations with gromacs, in *Solving Software Challenges for Exascale*, edited by S. Markidis and E. Laure (Springer International Publishing, Cham, 2015), pp. 3–27.

[29] T. Darden, D. York, and L. Pedersen, Particle mesh Ewald: An nlog(n) method for Ewald sums in large systems, J. Chem. Phys. **98**, 10089 (1993).

[30] S. Scherb, A. Hinaut, R. Pawlak, J. G. Vilhena, Y. Liu, S. Freund, Z. Liu, X. Feng, K. Müllen, T. Glatzel, A. Narita, and E. Meyer, Giant thermal expansion of a two-dimensional supramolecular network triggered by alkyl chain motion, Commun. Mater. **1**, 8 (2020).

[31] I. Cacelli and G. Prampolini, Parametrization and validation of intramolecular force fields derived from DFT calculations, J. Chem. Theory Comput. **3**, 1803 (2007).

[32] S. Kawai, M. Koch, E. Gnecco, A. Sadeghi, R. Pawlak, T. Glatzel, J. Schwarz, S. Goedecker, S. Hecht, A. Baratoff, L. Grill, and E. Meyer, Quantifying the atomic-level mechanics of single long physisorbed molecular chains, Proc. Natl. Acad. Sci. U.S.A. **111**, 3968 (2014).

[33] R. Pawlak, J. G. Vilhena, P. D'astolfo, X. Liu, G. Prampolini, T. Meier, T. Glatzel, J. A. Lemkul, R. Häner, S. Decurtins, A. Baratoff, R. Pérez, S. X. Liu, and E. Meyer, Sequential bending and twisting around C-C single bonds by mechanical lifting of a pre-adsorbed polymer, Nano Lett. **20**, 652 (2020).

[34] R. Pawlak, J. G. Vilhena, A. Hinaut, T. Meier, T. Glatzel, A. Baratoff, E. Gnecco, R. Pérez, and E. Meyer, Conformations and cryo-force spectroscopy of spray-deposited single-strand DNA on gold, Nat. Commun. **10**, 685 (2019).

[35] R. Pawlak, W. Ouyang, A. E. Filippov, L. Kalikhman-Razvozov, S. Kawai, T. Glatzel, E. Gnecco, A. Baratoff, Q. Zheng, O. Hod, M. Urbakh, and E. Meyer, Single-molecule tribology: Force microscopy manipulation of a porphyrin derivative on a copper surface, ACS Nano **10**, 713 (2016).

[36] N. Goga, A. J. Rzepiela, A. H. de Vries, S. J. Marrink, and H. J. C. Berendsen, Efficient algorithms for langevin and DPD dynamics, J. Chem. Theory Comput. **8**, 3637 (2012).